HHS Public Access

Author manuscript

Mater Sci Eng C Mater Biol Appl. Author manuscript; available in PMC 2020 April 01.

Published in final edited form as:

Mater Sci Eng C Mater Biol Appl. 2019 April ; 97: 784–792. doi:10.1016/j.msec.2018.12.113.

Multifunctional Nanoclusters of $NaYF_4$: Yb^{3+},Er^{3+} Upconversion Nanoparticle and Gold Nanorod for Simultaneous Imaging and Targeted Chemotherapy of Bladder Cancer

Suehyun K. Cho[a], **Lih-Jen Su**[b], **Chenchen Mao**[a], **Connor D. Wolenski**[a], **Thomas W. Flaig**[b], and **Wounjhang Park**[a,*]

[a]Department of Electrical, Computer, and Energy Engineering, University of Colorado, Boulder, CO 80309 U. S. A.

[b]Division of Medical Oncology, School of Medicine, University of Colorado Denver, 12801 E. 17th Ave. Aurora, CO 80045 U. S. A

Abstract

This paper reports successful synthesis of multifunctional nanoclusters of upconversion nanoparticle (UCNP) and gold nanorod (AuNR) through a PEGylation process. UCNPs emit visible luminescence under near-infrared excitation, producing high-contrast images with no background fluorescence. When coupled with AuNRs, the resulting UCNP-AuNR multifunctional nanoclusters is capable of simultaneous detection and treatment of bladder cancer. These UCNP-AuNR nanoclusters are further functionalized with antibodies to epidermal growth factor receptor (EGFR) to target bladder cancer cells known to overexpress EGFRs. This paper demonstrates, for the first time, efficient targeting of bladder cancer cells with UCNP-AuNR nanoclusters. In addition to high-contrast imaging and consequently high sensitivity detection of bladder cancer cells, highly selective optoporation-assisted chemotherapy was accomplished using a dosage of chemotherapy agent significantly lower than any previous reports, within a clinically relevant incubation window. These results are highly relevant to the eventual human application in which the nanoclusters and chemotherapy drugs will be directly instilled in bladder via urinary catheter.

Graphical Abstract

*Corresponding Author: Wounjhang Park, won.park@colorado.edu, Telephone: +1 303-735-3601, Fax: +1 303-492-2758.

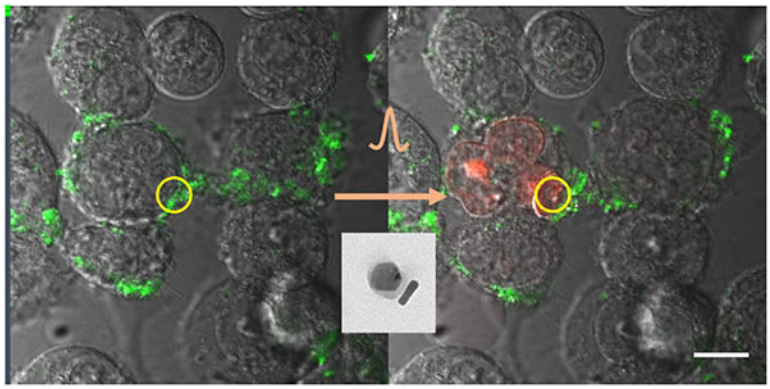

Keywords

Luminescence upconversion; Gold Nanorod; Surface Plasmon; Optoporation; Bladder Cancer

1. Introduction

Upconversion nanoparticles (UCNPs) have recently gained research interest due to several favorable characteristics. Because UCNPs upconvert lower energy photons in the near-infrared (NIR) region into higher energy photons in the visible, they provide distinct advantages of no autofluorescence, deeper tissue penetration, and minimal tissue damage.[1–5] Furthermore, the photophysical stability and higher upconversion efficiencies make them ideal for high-contrast, biological imaging.[6–9]

Earlier motivations of coupling plasmonic nanostructures with UCNPs have been mainly for upconversion enhancement using the enhanced local field of plasmon resonance.[10–15] However, achieving high enhancement in a controlled fashion in colloidal systems proved difficult and the focus has since shifted to achieving multimodal imaging and treatment.[5, 16–23] The coupling of UCNPs with Au nanoparticles for multimodal imaging and treatment has been demonstrated through several methods. Song et al. have grown upconversion shell on gold nanorods (AuNRs) and demonstrated upconversion imaging, magnetic imaging, and photothermal therapy.[16] Cheng et al. have grown an iron oxide shell and then subsequently a gold shell on top of UCNPs and demonstrated upconversion imaging, magnetic resonance imaging, and magnetic-field guided photothermal therapy.[17] He et al. have demonstrated coupling of UCNPs with various gold nanoparticles ranging from nanospheres to nanostars through the DNA-DNA binding. And with these nanoclusters, the authors have demonstrated multimodal imaging, photothermal therapy, and photodynamic therapy (PDT).[5] Sun et al. have coated their UCNPs with a combination of polyethylene glycol (PEG) and DNA to create a hierarchical AuNR and UCNP core-satellite nanoassemblies. The PEG was used to load Chlorin e6, a PDT agent and DNA was used to tether the UCNPs to the AuNRs. With these nanoclusters, the authors have demonstrated multimodal imaging, PDT, and photothermal therapy.[18] While various nanoclusters have demonstrated multifunctionality, no active targeting was present in the nanocluster and thus relied either on having prior information of the tumor location or on the enhanced permeability and retention (EPR) effect.

In this paper, we use a PEGylation based approach to create multifunctional nanoclusters of UCNPs and gold nanorods (UCNP-AuNR) which are bioconjugated with antibodies for targeted imaging and treatment of bladder cancer. Building on a previously reported method for UCNP functionalization, which uses a monofunctional amine-ended PEG as the hydrophilic end of their amphiphilic polymer,[24] we use a mixture of two different types of hydrophilic ends. Specifically, we mix heterofunctional amine and thiol functionalized PEG (NH_2-PEG-SH) with 2-methoxyethylamine (NH_2-EtOMe). Subsequently, this mixture is reacted with the hydrophobic poly(maleic anhydride-a/M-octadecene) (PMAO). This approach offers three distinct advantages. First, by using a heterofunctional NH_2-PEG-SH we have additional reactive thiol groups that will allow us to link UCNPs with gold through gold-thiol interaction. Second, we reduce particle aggregation more effectively by using a small molecule NH_2-EtOMe. Third, the reaction between PMAO and the amine group on PEG results in an additional carboxyl group that can be used for further functionalization with protein. Thus, we are able to conjugate the nanocluster with C-225, an antibody to epidermal growth factor receptor (anti-EGFR). With C-225 conjugation, the nanoclusters can actively target cancer cells by specifically binding with the epidermal growth factor receptors (EGFRs) that are known to be over-expressed on the bladder cancer cell membrane.[25, 26]

With the bioconjugated UCNP-AuNR nanoclusters, we demonstrate multimodal imaging and subsequent killing of bladder cancer cells through optoporation with sub-clinical dosage of chemotherapy agent. When irradiated by a femtosecond (fs) pulsed laser, nanobubbles are formed in the vicinity of the AuNRs and they subsequently disrupt the cell membrane upon irradiation.[27, 28] Using this optoporation technique, we porate the membranes of the EGFR expressing cancer cells, and therefore increase intake of sub-clinical dosage of cisplatin, a chemotherapy agent, to kill the cancer cells. To the best of our knowledge, (1) coupling of UCNPs and AuNRs through a PEGylation process and then functionalizing the nanoclusters with antibodies to actively target EGFR-expressing cancer cells to reduce treatment time to clinically relevant time frames, and (2) use of UCNPs in the nanoclusters, selectively bound to EGFR-positive cells, as imaging and detection agent in optoporation-assisted chemotherapy, have not been reported before. This active targeting does not rely on the EPR effect, which takes on the order of 24 hours for a significant accumulation of nanoparticles in tumor.[29] Instead, the incubation time can be drastically reduced down to 2 hours, as demonstrated later in this paper. We have also achieved effective cell killing with a dosage of chemotherapy agent much lower than what was previously reported. The eventual clinical application will involve direct installation of the nanoclusters in bladder for selective binding, followed by detection of cancer by UCNP fluorescence and subsequent optoporation-assisted chemotherapy with significantly reduced dosage. Therefore, the high contrast imaging, highly selective killing by optoporation-assisted chemotherapy and short incubation time are all critical requirements for successful clinical application.

2. Materials and methods

All the descriptions in Methods section are presented in further detail in the Supplementary Information. Briefly, we first synthesized UCNPs via thermal decomposition method[30] and AuNRs with seed-mediated growth method[31, 32] that have been previously reported. This

process uses NH_2-PEG-SH and NH_2-EtOMe to make PMAO amphiphilic. NH_2-PEG-SH provides thiols for further reaction with gold while the NH2-EtOMe acts as a stabilizer to minimize aggregation of the PEGylated UCNPs. Then, the coated UCNPs bind with AuNRs through the gold-thiol bonding process to create the UCNP-AuNR nanoclusters. The AuNRs used in this work have an average width of 11nm and length of 43nm and has a localized surface plasmon near 800nm (Supplementary Figure S1.) It is noted that the plasmon resonance is not matched with either absorption or emission of UCNP, as the primary goal of this work is not to enhance upconversion but to achieve multifunctionality - luminescence for imaging/detection and optoporation for therapeutics. Thus, we use small-size, detuned AuNRs for minimal luminescence quenching, which is demonstrated later.

The UCNP-AuNR nanoclusters were then functionalized with C-225, an antibody to epidermal growth factor receptor (EGFR). The amine end of the C-225 covalently bonds with the carboxylic end of the amphiphilic polymer to create an amide bond via the standard EDAC reaction, as described in the Supplementary Information.

Human bladder cancer cells are known to over-express EGFRs while normal urothelial cells don't.[25, 26] Thus, functionalization with anti-EGFR enables specific binding of the nanoclusters to bladder cancer cells. The selective binding of C-225 conjugated UCNP-AuNR nanoclusters was tested by treating with the UCNP-AuNR nanoclusters a mixture of EGFR-positive (A549) and EGFR-negative (H520) cells, a well-established model of EGFR expression.[33, 34] To distinguish EGFR-positive and EGFR-negative cells by conventional fluorescence microscopy, the EGFR-negative cells (H520) were developed by transducing NucLight Red lentivirus. The cells express nuclear restricted red fluorescent protein emitting at 633nm when excited by 588nm light, and thereby distinguishing themselves from the non-luminescent EGFR-positive (A549) cells. The presence of UCNP-AuNR nanoclusters was tested by the green fluorescence emitted by DyLight labelled secondary antibody against IgG, which we added to C-225 for convenient fluorescence detection. The DyLight luminescence is centered at 518nm upon blue excitation at 493nm.

Upconversion imaging of cells bound with UCNP-AuNR was performed with a Zeiss LSM 780 confocal microscope. The cells were illuminated by a Ti:Sapphire laser with center wavelength at 980nm. The collected signal was filtered to reject the 980nm laser and transmit only the visible luminescence.

Further confirmation of selective binding of nanoclusters was obtained by probing the optical signals arising from AuNRs. For this purpose, we prepared EGFR-negative (H520) and EGFR-positive (A549) cells separately and treated them with UCNP-AuNR nanoclusters. We then acquired infrared darkfield images in the NIR region. We used a conventional darkfield microscope setup with the addition of a 715nm longpass filter which blocks the innate scattered light from the cells in the visible while transmitting the increased scattering from AuNRs in the NIR.

For *in vitro* optoporation studies, different types of cells were seeded in 8-chamber coverglass system. Subsequently, the cells were incubated with C-225 or UNCP-AuNR for 2 hours and washed with phosphate-buffered saline (PBS) three times to remove unbound

nanoclusters. The incubated cells were then immersed in either Propidium iodide (PI) solution, PBS, or cisplatin during 800nm laser irradiation. Cell optoporation and cell death were monitored via conventional fluorescence microscopy.

3. Results

The synthesized UCNP-AuNR nanoclusters were examined via scanning electron microscopy (SEM) and transmission electron microscopy (TEM). A low magnification SEM image in Figure 1(a) shows a mixture of UCNP-AuNR nanoclusters and some excess AuNRs. Based on the TEM images from multiple regions, the yield of successful conjugation of the UCNP-AuNR nanocluster is estimated to be 34%, of which 59% is made of single AuNR and single UCNP (Supplementary Figure S2). Higher magnification TEM images shown in the inset of Figure 1 reveal a thin, uniform polymer coating on the UCNP surface, and AuNR attached to the surface of the PEGylated UCNP. To determine whether AuNRs quench upconversion PL of UCNPs, we performed a single nanoparticle PL spectroscopy. First, a diluted UCNPs and UCNP-AuNRs were dropcasted on a pattered Si substrate through the blade coating method. Then, by SEM, a single nanoparticle and a single nanocluster consisting of one UCNP and one AuNR were located. Afterwards, the upconverted PL from the single UCNP and single nanocluster was collected by a confocal microscope. As shown in Figure 1(b), there is no variations in the upconverted PL spectrum and intensity. This clearly shows that the upconverted luminescence is not adversely affected by the formation of UCNP-AuNR nanoclusters.

Figures 2(a)–(d) show results of this selective binding study. Figure 2(a) shows a brightfield image of a random mixture of A549 and H520 cells. When these cells are illuminated with 588nm light, the nuclei of the H520 (EGFR-negative) cells fluoresce in red, as demonstrated by Figure 2(b). When we switch the excitation light to blue, as in Figure 2(c), green luminescence is visible. This green fluorescence from the secondary antibody labeled with DyLight 488 visualizes the C-225 antibodies attached to the UCNP-AuNR nanoclusters. The overlay image of the red and green fluorescence with the brightfield image in Figure 3(d) shows no overlap between red and green fluorescence.

Next, we demonstrate the high-contrast upconversion luminescence imaging capability of the UCNP-AuNR nanoclusters. Figure 2(e) shows a brightfield image of T24T bladder cancer cells, an EGFR-positive cell line. Figure 2(f) and (g) show green and red PL, respectively, from the UCNPs upon 980nm excitation. The spectra of the green and red PL show characteristic PL spectra of UCNPs, providing direct evidence that UCNPs are bound on the membrane of these EGFR-positive cells. Unlike the conventional fluorescence imaging which typically accompanies substantial background autofluorescence, Figures 2(f) and (g) show high-contrast images with no background fluorescence. We further confirmed that the cells without UCNP-AuNR nanoclusters do not show any PL signal and thus the fluorescence image is completely black (data not shown).

Because cells are highly transparent in the NIR region, there is very little light scattering by the cells in the NIR region while AuNR scatters strongly due to the plasmon resonance. This can be observed in the micrographs shown in Figure 3(a) and (c), which are brightfield and

darkfield images of EGFR-negative cells (H520) treated with UCNP-AuNR nanoclusters, respectively. As can be seen in Figure 3(c), there is little scattering on the surface of H520 cells, indicating the absence of AuNRs and by extension UCNP-AuNR nanoclusters. In contrast, the EGFR-positive cells (A549) treated with UCNP-AuNRs show strong scattering in the NIR region. Figure 3(b) and (d) are brightfield and darkfield images, respectively, of the EGFR-positive cells (A549) treated with UCNP-AuNR nanoclusters. Figure 3(d) shows substantial scattered signals.

After confirming that the UCNP-AuNR nanoclusters have been successfully bound on the cell membranes, the optoporation capabilities were examined by irradiating the nanoclusters with fs laser pulses and subsequently monitoring the cells. The fs laser irradiation results in the formation of nano-/micro-scale bubbles around the plasmonic nanostructure by direct field ionization or strong local heating.[27, 28] This nano-cavitation process can disrupt the cell membrane and create nano-/micro-scale holes. To demonstrate the plasmon-mediated optoporation with our UCNP-AuNR nanoclusters, cells treated with and without UCNP-AuNR nanoclusters were irradiated with 100fs Ti:Sapphire laser at 800nm. Using a confocal microscope, we defined a small irradiation area (indicated by red squares in Figures 4(a)–(d)) and we irradiated the cells with a peak power density of 13MW cm^{-2} and a dwell time of 5μs for each pixel. The laser beam was scanned over the red square area twenty times. During the irradiation, the cells were immersed in a solution of propidium iodide (PI). PI does not normally enter the cells during incubation and remains non-fluorescent. But it emits red fluorescence when it reaches the cell nucleus. It is therefore an effective marker of cell membrane damage. In the experiments shown in Figures 4(a)–(d), all conditions including cell confluence, laser fluence, irradiation duration and area, were kept identical and the only variable was whether the cells were treated with UCNP-AuNR nanoclusters or not. We expected that the EGFR-positive HTB9 cells were bound with UCNP-AuNR nanoclusters and thus upon irradiation by fs laser pulses, their cell membrane should be compromised, allowing PI to enter the cell and reach the nucleus. At the nucleus, PIs bind with RNAs and become fluorescent which can be easily detected using a conventional fluorescence microscopy. Figure 4(a) and (b) show brightfield and fluorescence images, respectively, acquired 5min after the fs laser irradiation of HTB9 cells treated with UCNP-AuNR nanoclusters. Red fluorescence is clearly visible in Figure 4(b) indicating that the cell membrane has been compromised. On the other hand, Figure 4(c) and (d) show brightfield and fluorescence images, respectively, of HTB9 cells not treated with the nanoclusters. Under identical irradiation dosage and imaging conditions, no red fluorescence was observed in Figure 4(d). Since the selective binding of UCNP-AuNR nanoclusters to EGFR-positive cancer cells has already been demonstrated earlier, this result shows that we can selectively porate the cell membrane of the bladder cancer cells, opening the possibility of selectively delivering drugs to the targeted cancer cells.

We compared two different types of EGFR-positive bladder cancer cells (HTB9 and T24T) to quantify the effects of irradiation dosage on optoporation. We treated both cells with nanoclusters and irradiated them with fs laser pulses. As negative control, cells not treated with nanoclusters were also irradiated with the fs laser with the same conditions. PI was once again used to monitor the cell membrane damage. We varied the laser dosage and measured the area of poration by calculating the percentage of pixels within the irradiated

area that showed red fluorescence from PI. Figure 4(e) shows the area of cell poration as a function of total laser energy delivered to the cells. Both HTB9 and T24T cells, when treated with UCNP-AuNR nanoclusters, start exhibiting faint red PL starting at 13.8pJ. HTB9 shows a sharp increase in PL intensity at 15.9pJ and T24T at 16.2pJ. At 16.2pJ and 18.6pJ, respectively, HTB9 and T24T reach saturation where the porated area ceases to increase.

Simultaneous upconversion imaging and optoporation of UCNP-AuNR nanoclusters were performed by scanning the cells incubated with the nanoclusters with 980nm excitation. The green upconverted PL was imaged simultaneously with a brightfield image. As shown in Figure 4(f), we were able to identify the cells with nanoclusters by monitoring the upconverted PL intensities. We then irradiated only the region within the yellow circle five times with the fs laser (energy of 8pJ) and observed membrane disruption. Again, these experiments were conducted in PI solution to monitor the membrane compromise with PI fluorescence. Immediately following the fs laser irradiation, as depicted by Figure 4(g), the cell was enlarged and membrane disruption was visible at the location of laser irradiation. The subsequent penetration of PIs into the cell was visible 40s after the fs laser irradiation. At 16min after irradiation, we started to observe a bright fluorescence in the nuclei of the irradiated cell, indicating a successful penetration of PI, as shown in Figure 4(h).

Next, we conducted targeted drug delivery experiments utilizing optoporation mediated by UCNP-AuNR nanoclusters. Ideally, optoporation should only puncture small enough holes in the cell membrane that the cells can recover the following day. While porated, however, the drug intake by the cells is dramatically increased, enhancing the efficacy of the chemotherapy drugs. It is therefore possible to enable highly targeted chemotherapy by using optoporation mediated by the C-225 conjugated UCNP-AuNR nanoclusters. In this approach, targeted cancer cells are porated by UCNP-AuNRs and laser while the cells are simultaneously treated with a sub-clinical dosage of cisplatin, a chemotherapy drug. This way, only the porated cells will receive therapeutic dose while the unporated cells will remain unaffected.

To demonstrate the efficacy of the optoporation-based selective chemotherapy, we designed an experiment where we use sub-clinical dosages of cisplatin and monitored the cell viability 24 hours after irradiation. During the fs laser irradiation, the cells were left under one of the following conditions: (a) 200μL of 1.5μM of cisplatin in C-225 conjugated T24T cells (no UCNP-AuNR nanoclusters), (b) 200μL of PBS in UCNP-AuNR conjugated T24T cells, and (c) 200μL of 1.5μM of cisplatin in UCNP-AuNR conjugated T24T cells. An area of 2.656mm × 2.656mm was irradiated at $2.46 \times 10^7 \text{W cm}^{-2}$. The following day, the cells were imaged with 200μL of 0.5μg mL^{-1} of PI in PBS. Unlike in Figure 3 where the PI was used to examine the optoporation efficiency *in situ*, this time PI was used to quantify cell death. When PI is used during fs laser irradiation, it shows that the cell membranes are porated but it does not necessarily mean that the cells are killed. On the contrary, the cells generally recover the porated membranes in a day or so. When PI imaging is conducted 24 hours after the optoporation experiment, the cells are given sufficient time to recover from poration. Thus, the red fluorescence in this case signifies cell death, because the dead cells would not recover their cell membranes and thus the membranes remain compromised,

allowing the PI to penetrate the compromised membranes of the deal cells, reach the nuclei, bind with RNAs and fluoresce in red.

Figures 5(a)–(c) show an overlay of brightfield and fluorescence images of the three samples described above. As explained above, each cell that shows red fluorescence is a dead cell. Figure 5(a), where cells were irradiated with fs pulses in the presence of cisplatin but no UCNP-AuNR nanoclusters, the majority of cells remain alive as evidenced by the lack of fluorescence and high cell density. There is a small number of cells fluorescing in red, which is attributed to some local heating that leads to a marginal increase of cisplatin uptake.[39] In Figure 5(b), where the T24T cells were treated with UCNP-AuNRs but in the absence of cisplatin, we observed no PI fluorescence and the cell density remained high. This demonstrates that the cells that have UCNP-AuNR bound to their membranes and thus have been porated, recover fully when cisplatin is absent. When we have a combination of cisplatin and UCNP-AuNR nanoclusters during irradiation, however, we observed a significant decrease in cell viability. This can be seen by a larger number of PI stained cells and sparse cell density in Figure 5(c). When the cell viability was quantified (Figure 5(d)), we achieved cell viability below 20% with only 30min exposure of 1.5 μM of cisplatin when we utilize optoporation to enhance the chemotherapy drug intake. For further comparisons, we incubated the cells with varying concen trations of cisplatin from 1.65μM to 6.6μM for 72 hours and checked the long-term cell viability through an MTT assay (Figure 5(e)). We see that without the assistance of optoporation, T24T cells that have been incubated with 1.65 μM of cisplatin continuously for 72 hours exhibits 100% cell viability. This confirms that the 1.5 μM of cisplatin we used in the optoporation experiments is well below the lethal dosage. Even at 4.4 times higher concentration of cisplatin at 6.6μM we observed that the cell viability remains around 80%. Thus, with the highly specific cancer targeting possible with the C-225 conjugated UCNP-AuNR nanoclusters, we achieve highly targeted chemotherapy with drastically reduced damage to normal cells.

4. Discussion

The electron micrographs in Figure 1 demonstrate successful conjugation of UCNP-AuNRs. While the yield of 34% can be further improved in the future, we note that the unbound AuNRs present in our samples do not affect our experiments. This is because the C-225 antibodies are coupled through the carboxyl group present on the surface of UCNPs. Therefore, the unbound AuNRs do not have C-225 antibodies and are thus effectively removed during the rigorous washing processes we incorporated after incubation of the nanoclusters with the cells.

When coupling UCNPs with plasmonic structures, one must consider the interplay between the positive effect of surface plasmon resonance and the negative effects due to luminescence quenching and light scattering. It is well known that the presence of free electrons near a quantum emitter can effectively quench luminescence. In our UCNP-AuNR nanoclusters, the quenching effect should be minimal because we deliberately chose small size AuNRs. The small metal volume should naturally lead to less quenching. Additionally, light absorption and scattering by metal will reduce the intensity of the excitation laser that reaches UCNPs. Small metal volume reduces both light absorption and scattering, and thus

minimizes the negative effect on upconverted luminescence. Furthermore, we deliberately detuned the plasmon resonance of AuNRs from the UCNP absorption wavelength of 980nm so that the reduction of UCNP absorption should be minimal while the absorption at the plasmon resonance wavelength of 800nm remains strong enough to result in efficient optoporation. This is clearly shown by Figure 1(b).

The selective binding of UCNP-AuNRs to EGFR-positive cells is evidenced by the fluorescence micrographs in Figure 2 (a) – (d). The distinct red fluorescence from the nuclei of EGFR-negative cells and green fluorescence from the C-225 functionalized UCNP-AuNRs do not overlap. This is a clear evidence that the C-225 antibodies are only detected on the EGFR-positive cells. And since C-225 antibodies were conjugated onto UCNP-AuNR nanoclusters before they were incubated with the cell mixture, we can conclude that the UCNP-AuNRs are only bound to EGFR-positive cells and not to the EGFR-negative cells. This mixture of EGFR-positive and negative cells is a good representation of the *in vivo* situations where EGFR-positive cancer cells would be randomly distributed amid EGFR-negative normal cells. Furthermore, the upconversion PL images in Figure 2(e) – (h) show high-contrast uniform membrane binding of the UCNP-AuNR nanoclusters on the EGFR-positive cell membrane after 2 hours of incubation. Figure 2 therefore serves as a powerful evidence that the UCNP-AuNR nanoclusters will selectively bind only to the EGFR-expressing cancer cells in the eventual human application. While these images demonstrate selective binding of UCNP-AuNR nanoclusters on a macroscopic scale, more microscopic examinations of sparsely distributed EGFR-positive cells also show uniform membrane binding of UCNP-AuNR nanoclusters to EGFR-positive cells (Supplementary Figure S3.) We have also kept the cells (without any irradiation or treatment) incubated for 24 hours and performed upconversion imaging, which revealed all nanoparticles are taken up by the cells (Supplementary Figure S5). It is noted that membrane binding is sufficient for optoporation and endocytosis is not required. Much more important is the requirement of achieving dense membrane binding within 2 hours, which is considered the maximum time tolerated in intravesical therapy.

The darkfield micrographs depicting scattered light from AuNRs, in Figure 3, reiterate the selective binding of the nanoclusters to EGFR-positive cells. Because the darkfield images were acquired under identical irradiation and collection conditions, the increased scattering in Figure 3(d) is attributed to the increased scattering of incident irradiation due to the AuNRs present on the A549 cell membrane. The micrographs in Figure 3, taken with images in Figure 2 provide concrete evidence that UCNP-AuNR nanoclusters were successfully and selectively bound to the membrane of EGFR-positive cells.

The dosage-dependent optoporation shown in Figure 4 revealed different thresholds between two EGFR-positive cells (HTB9 and T24T) incubated with UCNP-AuNRs. The threshold of HTB9 cells were at a lower energy than that of T24T. We believe this difference occurs because HTB9 cells have higher EGFR expression than T24T cells and therefore have higher density of nanoclusters bound to their cell membranes.[29, 30] This is also consistent with the fact that the maximum porated area of HTB9 cells was larger than that of T24T cells. Once the laser power reaches 22.2pJ and 24.6pJ, respectively, HTB9 and T24T cells both started exhibiting nonspecific poration, as indicated by the increase in porated area in

the untreated cells. The decrease in PL area observed at even higher energies for the nanocluster conjugated cells is because the cells get deformed after irradiation and lose their original membrane integrities. While the details of optoporation results depend on the specific laser irradiation conditions and cell preparation conditions, our result shows that an optimum condition for selective optoporation can be achieved by properly adjusting the laser dosage. It is noted that the upconversion images in Figure 4(f)–(h) indicate incomplete membrane binding, which is due to the shorter incubation time (1.5 hours) used in these experiments. Our data show that membrane binding begins before 30 min and is complete by 2 hours of incubation (Supplementary Figure S6). For clinical applications, shorter incubation time is desirable and Figure 4 showa optoporation is possible with 90 min of incubation.

Finally, the effectiveness of optoporation-assisted chemotherapy was demonstrated. When the UCNP- AuNR treated cells are irradiated with fs pulsed laser, the ensuing nano-cavitation results in poration of cell membrane. By performing optoporation on the cells with a sub-clinical dosage of cisplatin, we show cell viability below 20% with just 30min of exposure while the same dosage has no cytotoxic effect on unporated cells. The effectiveness of our nanocluster is evident from the fact that effective cell killing was achieved with a much shorter incubation time and a substantially lower chemotherapy drug concentration than previous reports.[37 - 39] Both the shorter incubation time and lower dosage of chemotherapy drug are critical requirements for clinical applications because a lower dosage will reduce adverse side effects and 2 hours is known to be the longest intravescical treatment time tolerated in humans.

5. Conclusions

We demonstrate efficient coupling of UCNPs with AuNRs through a PEGylation process. The new PEGylation process allows the formation of highly stable UCNP-AuNR nanoclusters and further functionalization with antibodies for active targeting. In this work, we used C-225, antibody to EGFR for targeting bladder cancer cells. Thanks to the antibody interaction, we demonstrated that the C-225 antibody functionalized UCNP-AuNR nanoclusters uniformly bind to the EGFR-expressing cell membranes within 2 hours of incubation. This short incubation time is crucial for the future clinical application, as 2 hours is generally considered the longest intravesical treatment time tolerated in humans. Also, through upconversion photoluminescence imaging, we obtained high-contrast images showing selective binding of UCNP-AuNR nanoclusters to the EGFR-positive cancer cells and no binding to EGFR-negative cells. This provides evidence that these nanoclusters can be used for in situ detection of bladder cancer during a routine cystoscopic examination. Furthermore, we demonstrate an efficient and highly selective killing of the EGFR-positive cancer cells by utilizing optoporation-assisted chemotherapy. After 2 hours of incubation, cancer cells are detected by the UCNP fluorescence and, upon detection, treated immediately by the optoporation-assisted chemotherapy. When the UCNP-AuNR treated cells are irradiated with fs pulsed laser, the ensuing nano-cavitation results in poration of cell membrane. By performing optoporation on the cells with a sub-clinical dosage of cisplatin, we show cell viability below 20% with just 30 min of exposure while the same dosage has no cytotoxic effect on unporated cells. This approach allows us to use minimal

chemotherapy agent and thus minimize the negative side effects for the patients, while obtaining pronounced therapeutic effect on the targeted cancer cells.

This paper shows a realistic pathway to clinical application in which the UCNP-AuNR nanoclusters are directly instilled in bladder via urethral catheterization. In particular, there are two distinct advantages over previously reported multifunctional nanoclusters. First, we demonstrate a unique treatment method of optoporation-assisted chemotherapy, guided by upconversion imaging. Unlike photothermal ablation techniques, whose performance can be affected by local heat dissipation conditions, we utilize local optoporation in the presence of significantly lower dosage and exposure time of cisplatin, a conventional chemotherapy agent. Second, we demonstrate an effective killing of EGFR-positive cells within a clinically relevant time frame. Active targeting of UCNP-AuNR nanoclusters results in selective binding of the nanoclusters specifically to EGFR-positive cells within 2 hours of incubation, which is a maximum duration allowed for intravesical treatment tolerated in humans.

Supplementary Material

Refer to Web version on PubMed Central for supplementary material.

Acknowledgements

This work was supported in part by the National Science Foundation [DMR-1420736, MRSEC: Soft Materials Research Centre], the Army Research Office [W911NF-14-1-0211, W911NF-14-1-0463], National Institute of Health [1R21EB020911-01] and the Colorado Office of Economic Development & International Trade [CTGG1 2017-0609].

Abbreviations:

UCNP	Upconversion nanoparticle
AuNR	Gold nanorods
PDT	Photodynamic therapy
PEG	Polyethylene glycol
EPR	Enhanced permeability and retention
EGFR	Epidermal growth factor receptor
NH_2-PEG-SH	Heterofunctional amine and thiol functionalized PEG
NH_2-EtOMe	2-methoxyethylamine
PI	Propidium iodide
PBS	phosphate-buffered saline
PL	Photoluminescence

References

[1]. Auben JE Autofluorescence of viable cultured mammalian cells. J. Histochem. Cytochem 1979, 27, 36–43. [PubMed: 220325]

[2]. Bashkatov AN; Genina EA; Kuchovev VI; Tuchin VV Optical properties of human skin, subcutaneous and mucous tissues in the wavelength range from 400 to 2000 nm. J. Phys. D: Appl. Phys 2005, 38, 2543–2555.

[3]. Chatterjee DK; Yong Z Upconverting nanoparticles as nanotransducers for photodynamic therapy in cancer cells. Nanomedicine 2008, 3, 73–82. [PubMed: 18393642]

[4]. Konig K; So PT; Mantulin WW; Tromberg BJ; Gratton E Two-photon excited lifetime imaging of autofluorescence in cells during UVA and NIR photostress. J. Microsc 1996, 183, 197–204. [PubMed: 8858857]

[5]. He L; Dragavon J; Cho S; Mao C; Yildirim K; Ma K; Chatteraj R; Goodwin AP; Park W; Cha JSelf-assembled gold nanostar-$NaYF_4$:Yb/Er clusters for multimodal imaging, photothermal and photodynamic therapy. J. Mater. Chem. B 2016, 4, 4455–4461.

[6]. Deng M; Ma Y; Huang S; Hu G; Wang L Monodisperse upconversion NaYF4 nanocrystals: Syntheses and bioapplications. Nano Res. 2001, 4, 685–694.

[7]. Wu S; Han G; Milliron DJ; Aloni S; Altoe V; Talapin DV; Cohen BE; Schuck PJ Non-blinking and photostable upconverted luminescence from single lanthanide-doped nanocrystals. P. Natl. Acad. Sci 2009, 106, 10917–10921.

[8]. Ostrowski AD; Chan EM; Gargas DJ; Katz EM; Han G; Schuck PJ; Milliron DJ; Cohen BE Controlled synthesis and single-particle imaging of bright, sub-10 nm lanthanide-doped upconverting nanocrystals. ACS Nano 2012, 6, 2686–2692. [PubMed: 22339653]

[9]. Auzel F Upconversion and anti-Stokes processes with f and d ions in solids. Chem. Rev 2004, 104, 139–173. [PubMed: 14719973]

[10]. Saboktakin M; Ye X; Oh SJ; Hong S-H; Fafarman AT; Chettiar UK; Engheta N; Murray CB; Kagan CRMetal-enhanced upconversion luminescence tunable through metal nanoparticle-nanophosphor separation. ACS Nano 2012, 6, 8758–8766. [PubMed: 22967489]

[11]. Priyam A; Idris NM; Zhang Y Gold nanoshell coated NaYF4 nanoparticles for simultaneously enhanced upconversion fluorescence and darkfield imaging. J. Mater. Chem 2012, 22, 960–965.

[12]. Lu D; Cho SK; Ahn S; Brun L; Summer CJ; Park W Plasmon enhancement mechanism for the upconversion processes in $NaYF_4$:Yb^{3+},Er^{3+} nanoparticles: Maxwell versus Forster. ACS Nano 2014, 8, 7780–7792. [PubMed: 25003209]

[13]. Lu D; Mao C; Cho SK; Ahn S; Park W Experimental demonstration of plasmon enhanced energy transfer rate in $NaYF_4$:Yb^{3+},Er^{3+} upconversion nanoparticles. Sci. Rep 2016, 6, 18894. [PubMed: 26739230]

[14]. Park W; Lu D; Ahn S Plasmon enhancement of luminescence upconversion. Chem. Soc. Rev 2015, 44, 2940–2962. [PubMed: 25853439]

[15]. Schietinger S; Aichele T; Wang HQ; Nann T Plasmon-enhanced upconversion in single $NaYF_4$:Yb^{3+}/Er^{3+} Codoped Nanocrystals. Nano Lett 2010, 10, 134–138. [PubMed: 20020691]

[16]. Song Y; Liu G; Dong X; Wang J; Yu W; Li J Tunable multicolor upconversion emissions and paramagnetic property of monodispersed bifunctional lanthanide-doped $NaGdF_4$ nanorods. J. Phys. Chem. C 2011, 119, 18527–18536.

[17]. Cheng L; Yang K, Li Z; Zheng X; Shao M; Lee S-T; Liu ZMultifunctional nanoparticles for upconversion luminescence/MR multimodal imaging and magnetically targeted photothermal therapy. Biomaterials 2011, 33, 2215–2222. [PubMed: 22169825]

[18]. Sun M; Xu L; Wu X; Kuang H; Wang L; Xu C Hierarchical plasmonic nanorods and upconversion core-satellite nanoassemblies for multimodal imaging-guided combination phototherapy. Adv. Mater 2016, 28, 898–904. [PubMed: 26635317]

[19]. Li D; Lai W-Y; Shao Q; Huang WMultifunctional NaYF4:Yb3+,Er3+@SiO2@Au heterogeneous nanocomposites for upconversion luminescence, temperature sensing and photothermal conversion. RSC Adv. 2017, 7, 11491

[20]. Chen H; Guan Y; Wang S; Ji Y; Gong M; Wang L Turn-on detection of a cancer marker based on near-infrared luminescence energy transfer from NaYF4:Yb,Tm/NaGdF4 core-shell upconverting nanoparticles to gold nanorods. Langmuir 2014, 30, 13085–13091. [PubMed: 25296290]

[21]. Huang Y; Rosei F; Vetrone F A single multifunctional nanoplatform based on upconversion luminescence and gold nanorods. Nanoscale 2015, 7, 5178. [PubMed: 25699524]

[22]. Qian LP; Zhou LH; Too H-P; Chow G-M Gold decorated NaYF4:Yb,Er/NaYF4/silica (core/shell/shell) upconversion nanoparticles for photothermal destruction of BE(2)-C neuroblastoma cells. J. Nanopart Res 2011, 13, 499–510.

[23]. Zhang Y; Chen B; Xu S; Li X; Zhang J; Sun J; Zheng H; Tong L; Sui G Zhong H; Xia H; Hua R Dually functioned core-shell NaYF4:Er3+/Yb3+@NaYF4:Tm3+/Yb3+ nanoparticles as nanocalorifiers and nano-thermometers for advanced photothermal therapy. Sci. Rep 2017, 7, 11849. [PubMed: 28928385]

[24]. Wang C; Cheng L; Liu Z Drug delivery with upconversion nanoparticles for multi-functional targeted cancer cell imaging and therapy. Biomaterials 2011, 32, 1110–1120. [PubMed: 20965564]

[25]. Rotterud R; Nesland JM; Berner A; Fossa SD Expression of the epidermal growth factor receptor family in normal and malignant urothelium. BJUInt. 2005, 95, 1344–1350.

[26]. Popov Z; Gil-Diez-de-Medina S; Ravery V; Hoznek A; Bastuji-Garin S; Lefrere-Belda A; Abbou CC; Chopin DK Prognostic value of EGF receptor and tumor cell proliferation in bladder cancer: therapeutic implications. Urol. Oncol 2004, 22, 93–101. [PubMed: 15082004]

[27]. Boulais E; Lachaine R; Meunier M Plasma-mediated nanocavitation and photothermal effects in ultrafast laser irradiation of gold nanorods in water. J. Phys. Chem. C 2013, 117(18), 9386–9396.

[28]. Bergeron E; Boutopoulos C; Martel R; Torres A; Rodriguez C; Niskanen J; Lebrun J-J; Winnik FM; Sepieha P; Meunier M Cell-specific optoporation with near-infrared ultrafast laser and functionalized gold nanoparticles. Nanoscale 2015, 7, 17836. [PubMed: 26459958]

[29]. Miao L; Guo S; Zhang J; Kim WY; Huang L Nanoparticles with precise ratiometric co-loading and co-delivery of gemcitabine monophosphate and cisplatin for treatment of bladder cancer. Adv. Funct. Mater 2014, 24, 6601–6611. [PubMed: 25395922]

[30]. Li Z; Zhang Y An efficient and user-friendly method for the synthesis of hexagonal-phase $NaYF_4$:Yb,Er/Tm nanocrystals with controllable shape and upconversion fluorescence. Nanotechnol. 2008, 19, 345606.

[31]. Nikoobakht B; A. El-Sayed MA Preparation and growth mechanism of gold nanorods (NRs) using deed-mediated growth method. Chem. Mater 2003, 15, 1957–1962.

[32]. Cho SK; Emoto K; Su L-J; Yang X; Flaig TW; Park WFunctionalized gold nanorods for thermal ablation treatment of bladder cancer. J. Biomed. Nanotechnol 2014, 10, 1–10. [PubMed: 24724494]

[33]. Yang X; Su L-J; La Rosa FG; Smith EE; Schlaepfer IR; Cho SK; Kavanagh B; Park W; Flaig TWThe antineoplastic activity of photothermal ablative therapy with targeted gold nanorods in an orthotopic urinary bladder cancer model. Bladder Cancer 2017, 3, 201–210. [PubMed: 28824948]

[34]. Tang Z; Du R; Jiang S; Wu C; Barkauskas DS; Richey J; Molter J; Lam M; Flask C; Gerson S; Dowlati A; Liu L; Lee Z; Halmos B; Wang Y; Kern JA; Ma PC Dual MET-EGFR combinatorial inhibition against T790M-EGFR-mediated erlotinib-resistant lung cancer. Brit. J. Cancer 2008, 99, 911–922. [PubMed: 19238632]

[35]. Yang X; Kessler E; Su L-J; Thorburn A; Frankel AE; Li Y; Varella-Garcia M; Glode LM; Flaig TWDiphtheria toxin-epidermal growth factor fusion protein DAB389EGF for the treatment of bladder cancer. Clin. Cancer Res 2013, 19, 148–157. [PubMed: 23172881]

[36]. Railkar R; Krane LS; Li QQ; Sandford T; Siddiqui MR; Haines D; Vourganti S; Brancato SJ; Choyke PL; Kobayashi H; Agarwal PK Epidermal growth factor receptor (EGFR)-targeted photoimmunotherapy (PIT) for the treatment of EGFR-expressing bladder cancer. Mol. Cancer Ther 2017, 16, 2201–2214. [PubMed: 28619755]

[37]. Ohno S; Siddik ZH; Kido Y; Zwelling LA; Bull JMCThermal enhancement of drug uptake and DNA adducts as a possible mechanism for the effect of sequencing hyperthermia on cisplatin-induced cytotoxicity in L1210 cells. Cancer Chemoth. Pharm 1994, 34, 302–306.

[38]. Lukianova-Hleb EY; Ren X; Zasadzinski JA; Wu X; Lapotko DO Plasmonic nanobubbles enhance efficacy and selectivity of chemotherapy against drug-resistant cancer cells. Adv. Mater 2012, 24, 3831–3837. [PubMed: 22407874]

[39]. Lukianova-Hleb EY; Belyanin A; Kashinath S; Wu X; Lapotko DO Plasmonic nanobubble-enhanced endosomal escape processes for selective and guided intracellular delivery of chemotherapy to drug-resistant cancer cells. Biomaterials 2012, 33, 1821–1826. [PubMed: 22137124]

Highlights

- Multifunctional nanoclusters made of upconversion nanoparticle and plasmonic nanoparticle enable simultaneous detection and treatment of cancer
- Upconversion nanoparticles allow high sensitivity fluorescence detection of cancer cells
- Plasmonic aided optoporation of cancer cells enable highly selective chemotherapy
- Efficient cell binding and optoporation-enabled chemotherapy was demonstrated within a clinically relevant time scale.

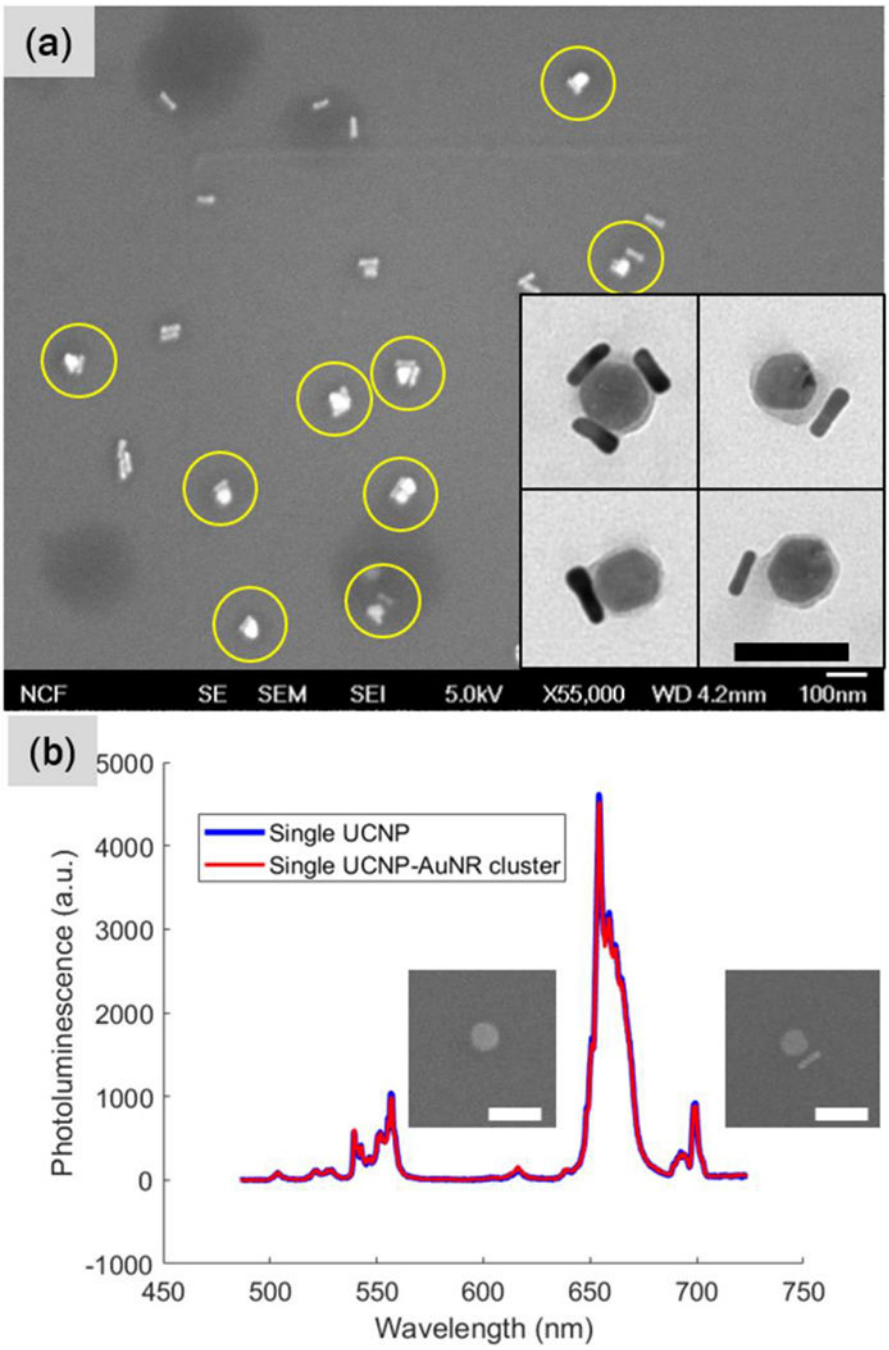

FIGURE 1.

(a) Electron microscopy images of UCNP-AuNR nanoclusters. A low magnification SEM image reveals successful UCNP-AuNR conjugation yield of 33.6%. The inset shows higher magnification TEM images of the UCNP-AuNR clusters. Scale bars indicate 100 nm. The average diameter of UCNPs is 48.2 ± 5.17nm. (b) Upconversion PL spectra of single UCNP and UCNPAuNR nanocluster consisting of one UCNP and one AuNR. There is no significant PL quenching due to the addition of a single AuNR. Scale bar indicates 100nm. The average diameter of UCNPs is 48.2 ± 5.17nm. (b) Upconversion PL spectra of single

UCNP and UCNP-AuNR nanocluster consisting of one UCNP and one AuNR. There is no significant PL quenching due to the addition of a single AuNR. Scale bar indicates 100nm.

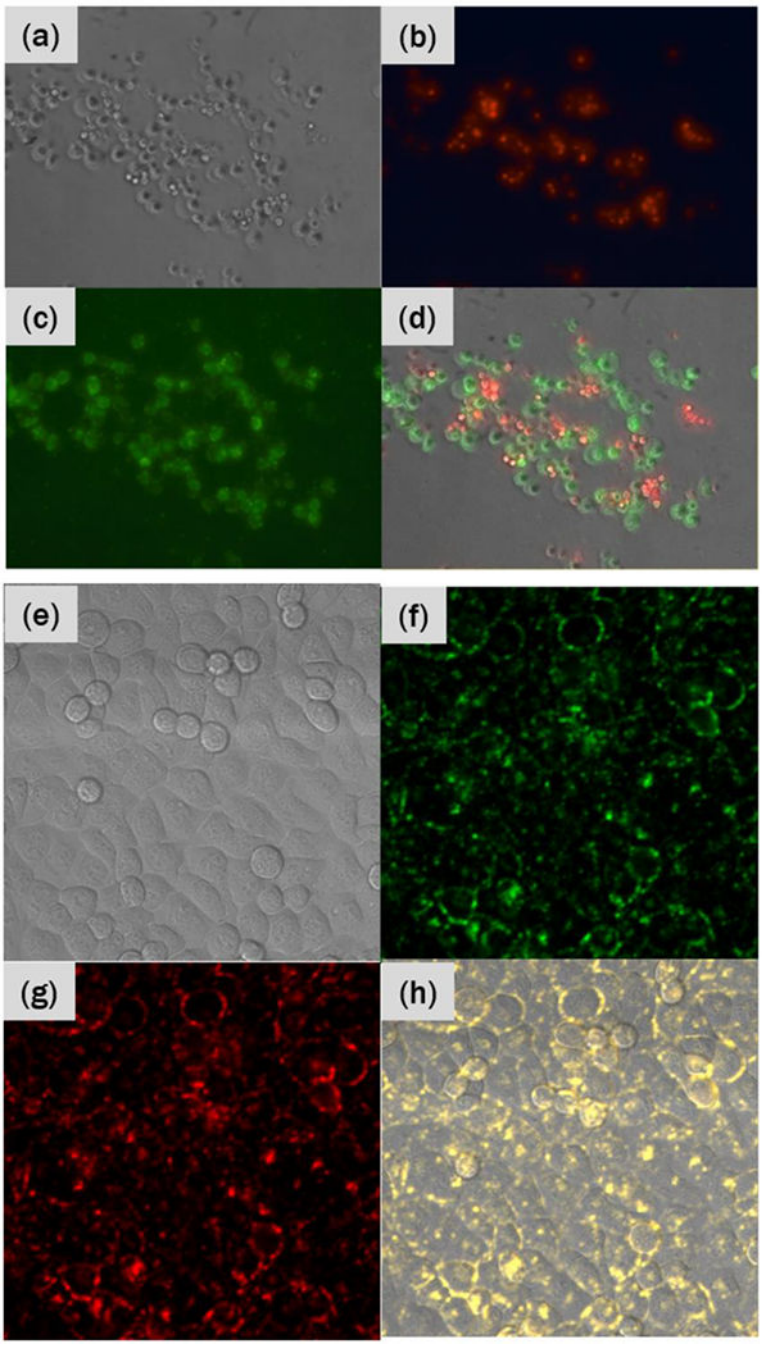

FIGURE 2.

(a) Brightfield image of a mixture of A549 (EGFR-positive) and H520 (EGFRnegative) cells. (b) Red fluorescence image showing luminescence from the nuclei of H520 cells and (c) green fluorescence image showing luminescence from the C-225 antibodies conjugated on UCNP-AuNR nanoclusters. (d) An overlay of both fluorescence images with the brightfield image. (e) Brightfield image of T24T cells conjugated with UCNP-AuNR nanoclusters. Confocal mapping of PL signal upon 980nm excitation in (f) green and (g) red.

(h) An overlay of green and red PL maps with the brightfield image shows membrane binding, with yellow representing dual green and red detection.

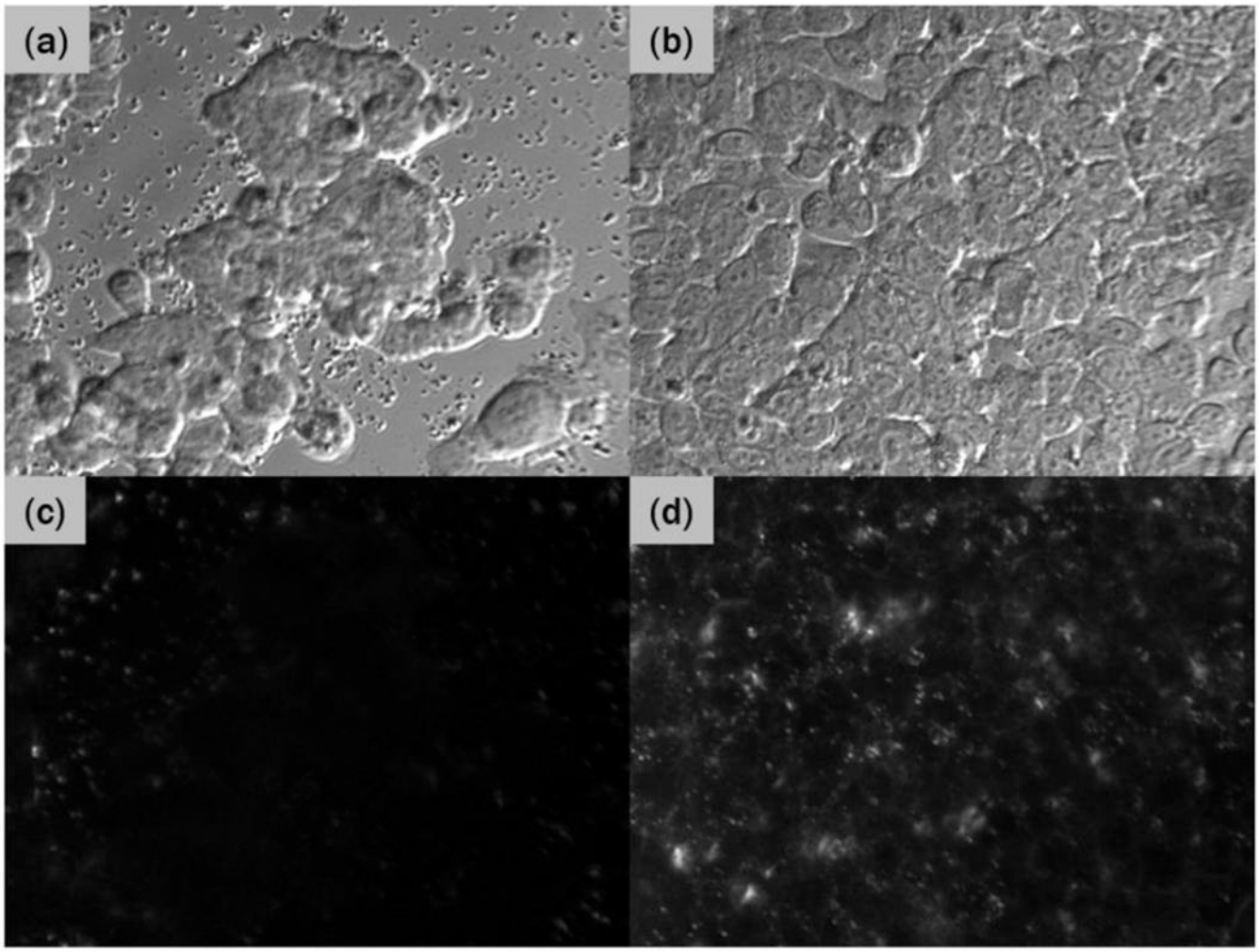

FIGURE 3.
Brightfield images of (a) EGFR-negative (H520) cells and (b) EGFR-positive (A549) cells. (c) and (d) show the corresponding NIR darkfield images of cells incubated with UCNPAuNR nanoclusters and then washed off with PBS.

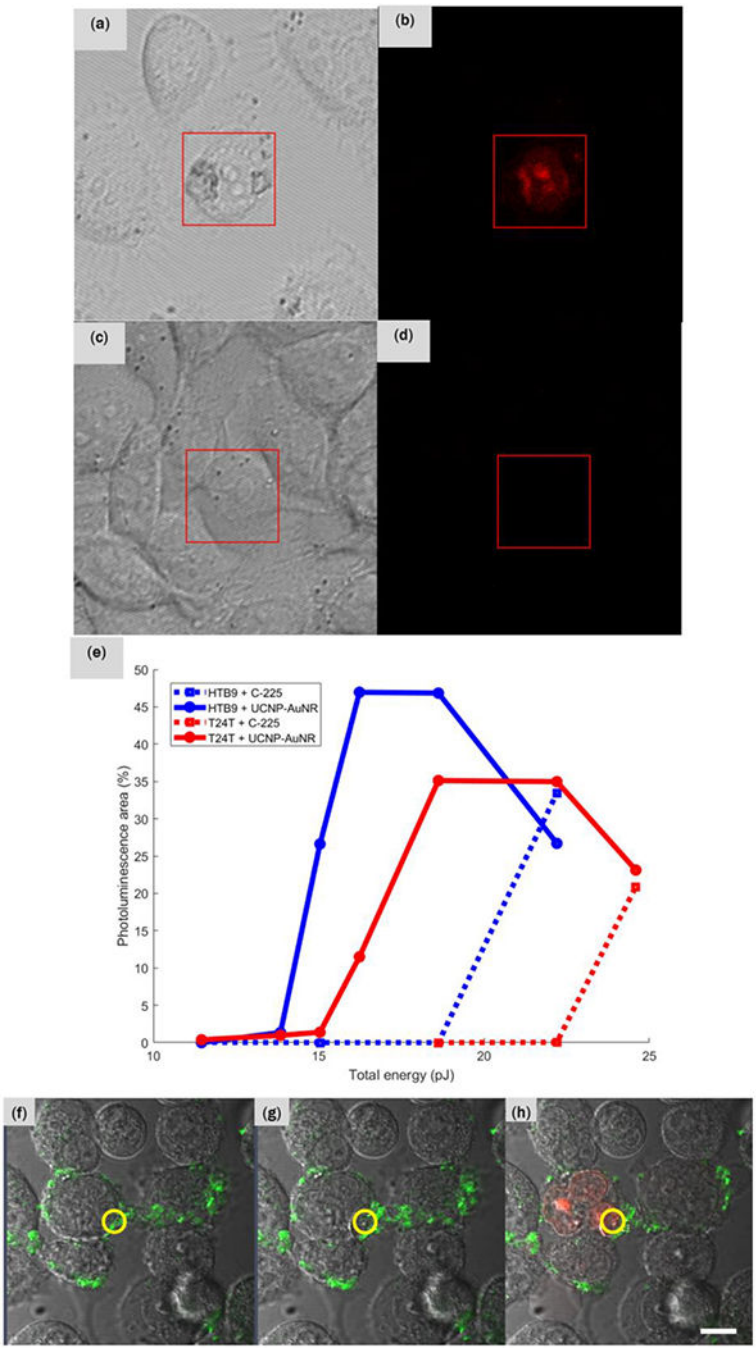

FIGURE 4.

(a) Brightfield and (b) corresponding red fluorescence micrograph of HTB9 cells bound with UCNP-AuNR nanoclusters. (c) Brightfield and (d) corresponding red fluorescence micrographs of HTB9 cells without the nanoclusters. Both sets of samples have been irradiated with identical dosage of fs laser and all images were acquired 5 min after irradiation. (e) Quantification of percentages of pixel exhibiting red fluorescence in both HTB9 and T24T cells with and without UCNP-AuNR conjugation with respect to total energy delivered to the cells. (f) T24T cells bound with UCNP-AuNR nanoclusters. Green

signal is the upconverted PL from the UCNPs present on the cell membrane. The irradiation occurred only within the red circular region. (g) T24T cells immediately after the fs pulse irradiation shows membrane disruption and cell enlargement (time lapse video is also available), and (h) 16 min after the fs pulse irradiation, red fluorescence was visible within the cell nuclei indicating that the PI dye penetrated through the porated cell membrane and reacted with RNA within the nuclei. The scale bar indicates 10 μm.

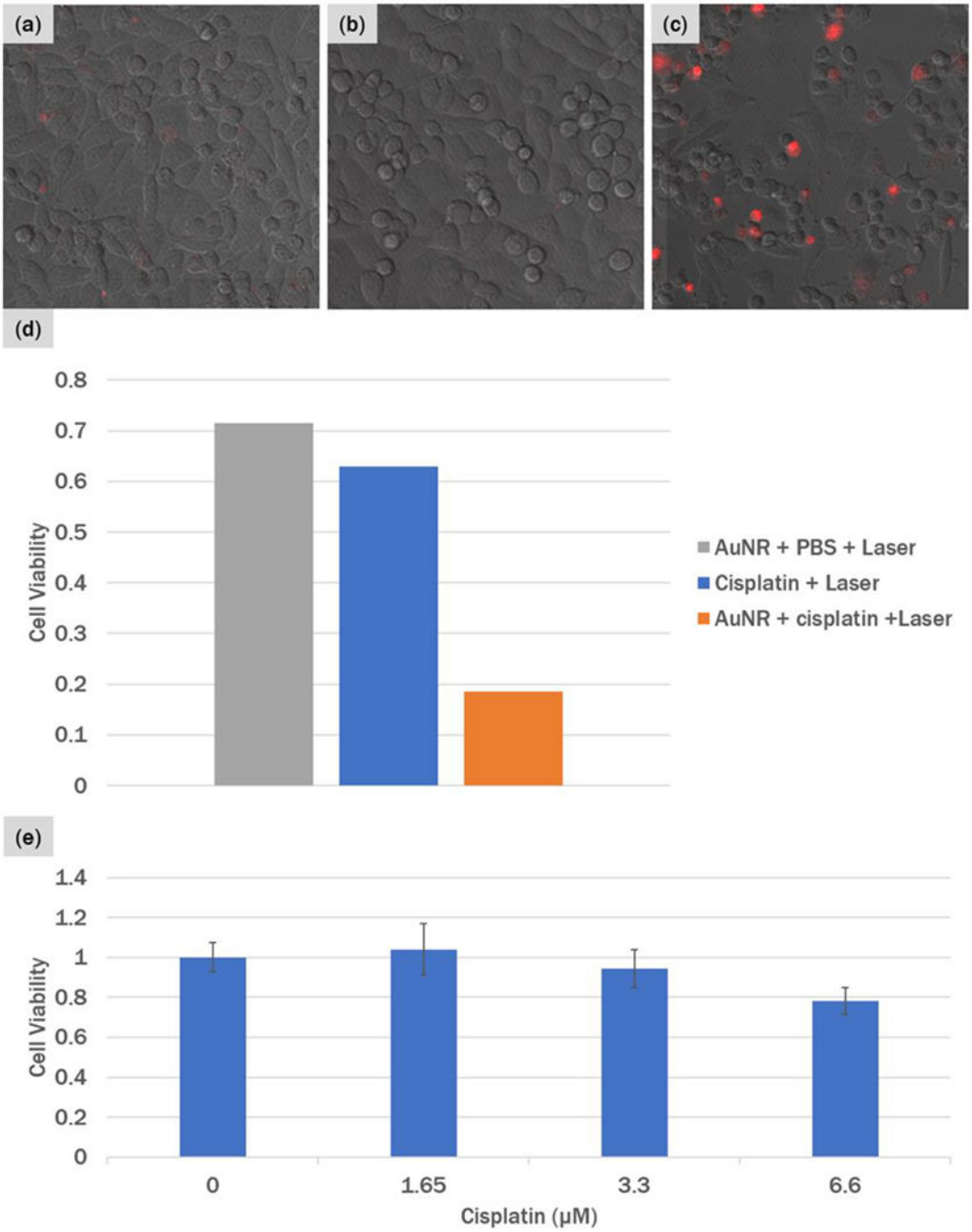

FIGURE 5.

PI staining of cells 24 hours after irradiation. (a) T24T cells incubated with 1.5 μM of cisplatin and irradiated with the fs laser, (b) T24T cells conjugated with UCNP-AuNR nanoclusters and irradiated with fs laser in PBS, and (c) T24T cells conjugated with UCNP-AuNR nanoclusters and irradiated with fs laser in the presence of 1.5 μM of cisplatin. (d) Calculated cell viability compared to unirradiated region and (d) control cell viability of T24T cells with various dosages of cisplatin incubated for 72 hours.